Colloid & Polymer Science Colloid Polym Sci 272:1344–1351 (1994)

Time-resolved SAXS studies of morphological changes in cold crystallized poly(ethylene terephthalate) during annealing and heating*)

A. M. Jonas[1]), T. P. Russell, and D. Y. Yoon

IBM Almaden Research Center, San Jose, California, USA
[1]) Present Address: Laboratoire des Hauts Polymères; Université Catholique de Louvain; Place Croix du Sud, 1; B-1348 Louvain-la-Neuve; Belgium (E.U.)

*) *Dedicated to Prof. E. W. Fischer on the occasion of his 65th birthday.*

Abstract: Structural changes occurring during crystallization of quenched amorphous poly(ethylene terephthalate) (PET) and subsequent cooling/heating cycles have been studied by real-time small-angle x-ray scattering (SAXS), using synchrotron radiation. Initial crystallization is found to occur by insertion of new lamellae between the existing ones, while rapid continuous melting/recrystallization happens when the cold-crystallized PET samples are heated above the previous highest annealing temperature. Such melting/recrystallization results in irreversible increases in the lamellar long period, the crystal thickness and the density difference between the crystalline and amorphous regions; in contrast, at temperatures below the prior highest crystallization temperature, the structural changes are dominated by reversible effects such as thermal expansion. However, throughout the entire temperature range up to the melting point around 250 °C, the crystal core thickness remains quite small, less than ca. 50 Å, and the linear crystallinity of lamellar stacks remains nearly constant around 0.3. Such a low crystallinity indicates the presence of thick order-disorder interfacial layers on the lamellar surface, whose thickness increases with temperature.

Key words: Poly(ethylene terephthalate) – lamellar morphology – melting-recrystallization – annealing

Introduction

The morphology of semi-crystalline polymers is known to depend on their thermal history. In this respect, understanding the evolution of the structure due to any thermal treatment performed after the crystallization is of practical and fundamental importance, in order to properly interpret data from thermal analyses (differential scanning calorimetry (DSC), dielectric and mechanical spectroscopies, etc.) as well as to optimize processing conditions. It is also a prerequisite to the scientific understanding of the crystallization of polymers in general.

In a previous paper [1], an extensive structural characterization was presented on the crystallization and subsequent thermal evolution of cold-crystallized poly(ether-ether-ketone) (PEEK) and of its blends with poly(ether imide), by means of small-angle and wide-angle x-ray scattering measurements performed in real time using synchrotron radiation. It was shown that isothermal crystallization from the glass proceeds by an insertion mechanism whereby lamellae of almost identical thicknesses are progressively inserted between existing lamellae. Samples crystallized or annealed at T_c underwent a melting-recrystallization process when heated above T_c. This process is characterized by an irreversible increase of the crystal thickness, of the distance between the crystals, and of the perfection and average density of the crystals. When the polymer is cooled below

T_c, the structural parameters change reversibly. This results from thermal expansion and reversible variations of strains in the crystals. Some of these observations were in agreement with previous real-time studies performed on cold-crystallized PEEK or other aromatic polymers [2–8]. For instance, the existence of a melting-recrystallization mechanism has been shown by Gehrke et al. [4] for cold-crystallized poly(ethylene terephthalate) (PET), in agreement with the usual interpretations of the DSC scans of such samples [9, 10]. The insertion mechanism occurring during the crystallization of aromatic polymers has also been supported by others [2, 3, 5–7].

The aim of the present paper is to investigate whether the conclusions drawn for PEEK are also applicable for another aromatic polymer, PET. This would lend some credence to the idea that the crystallization and subsequent structural evolution of aromatic polymers are governed by identical mechanisms. Hence, cyclic heating/cooling experiments, similar to those previously performed on PEEK [1], have been carried out on PET, while recording the small-angle x-ray scattering (SAXS) of the sample in real time. The main focus of the study will thus be on the structural evolution that follows initial crystallization, rather than on the initial crystallization itself.

Experimental

Materials

The PET powder was obtained from Polysciences, Inc. The molecular masses were determined by size-exclusion chromatography to be 9800 for number average M_n and 19 900 for weight average M_W, respectively. The powder was compression-molded at 280 °C for 10 min to obtain $\sim 400\ \mu m$ thick films. The films were directly quenched in water from the processing temperature to room temperature. The quenched films were clear and transparent, with no voids.

Differential scanning calorimetry (DSC)

The DSC thermograms were obtained with a Perkin-Elmer DSC7, calibrated with Indium and Zinc.

Small-angle X-ray scattering (SAXS)

SAXS measurements were performed on beamline I-4 at the Stanford Synchrotron Radiation Laboratory (SSRL), in transmission geometry. The temperature of the sample was controlled by a Mettler hot stage operating between 50° and 300 °C. Heating and cooling rates were set to 3 °C min^{-1}. The acquisition time for each scattering curve was 1 min. The data were corrected for instrumental effects as described elsewhere [11]. No desmearing was performed, given the high collimation of the beam and its very small cross-section. Because of the limited angular range probed, a simple constant background was subtracted from the data.

The following parameters have been extracted from the data:

1) the long period (L), i.e., the average distance between crystals in the fibrils of the spherulites, from the maximum of the Lorentz-corrected SAXS interference peak.

2) the invariant (Q), i.e., the integral over reciprocal space of the intensity scattered in the SAXS range. For an isotropic sample with a linear density profile of thickness d accommodating the density difference between the crystalline and amorphous regions (density transition layer):

$$\begin{aligned} Q &= K \int_0^\infty q^2 I_{\mathrm{SAXS}}(q)\,dq \\ &\propto \phi_s\left(\phi_{c,\mathrm{lin}}(1-\phi_{c,\mathrm{lin}}) - \frac{d}{3L}\right)(\rho_c - \rho_a)^2 \\ &\tilde{\propto}\ \phi_s(\phi_{c,\mathrm{lin}}(1-\phi_{c,\mathrm{lin}}))(\rho_c - \rho_a)^2\,, \end{aligned} \tag{1}$$

where $q = 4\pi \sin(\theta)/\lambda$ is the magnitude of the scattering vector; 2θ is the scattering angle; λ is the wavelength; and K is a constant. ϕ_s is the volume fraction of lamellar stacks, $\phi_{c,\mathrm{lin}}$ is the linear crystallinity (i.e., the relative volume fraction of crystalline lamellae in the lamellar stacks) and ρ_i is the electron density of phase i. Within this model, the sample is approximated as an assembly of stacks made of alternating crystalline and amorphous layers. Such an approximation is valid because, given the wavelengths used, the SAXS signal is dominated by the scattering of these stacks (= fibrils of the real spherulites). The total sample crystallinity is simply $\phi_s\phi_{c,\mathrm{lin}}$. Since the data have not been calibrated in absolute

units, Q has only a qualitative meaning in this paper.

3) the average lamellar thickness L_c and the linear crystallinity $\phi_{c,lin}$. L_c is obtained from the one-dimensional correlation function ($\gamma_1(r)$), computed by Fourier transformation of the Lorentz-corrected scattering extrapolated using an extended Porod's law [12]. Rigorously, a prior knowledge of the linear crystallinity is required to determine accurately the values of L_c from the correlation function [13]. However, a reasonable estimation of L_c can be obtained by computing the distance r corresponding to the intersection between the slope of the self-correlation triangle with the horizontal line passing through the first minimum of the correlation function [13]. Then, from the ratio of L_c and L, one obtains an estimation for $\phi_{c,lin}$.

It should be stressed that the evaluation of L_c and $\phi_{c,lin}$ are only approximate. First, it has been shown [14, 15] by transmission electron microscopy that the lateral sizes of PET lamellae are very restricted for annealing temperatures lower than 180 °C. This raises questions on the validity of the Lorentz correction or of a one-dimensional correlation function for analyzing the scattering data from samples annealed at these temperatures. Moreover, no correction for the existence of density transition layers has been performed on $\gamma_1(r)$. However, this is not likely to introduce much error, since it has been demonstrated that the density transition layers are of very limited spatial extent in semi-crystalline PET [16–18]. Finally, the estimation procedure itself tends to slightly underestimate L_c and $\phi_{c,lin}$. Given the approximations involved, the precisions on L_c and $\phi_{c,lin}$ are thus not expected to be better than about 20%. Nevertheless, despite these limitations, it is possible to extract general trends from this simple analysis.

Another problem connected to the evaluation of L_c is that there is no way to determine solely by SAXS whether the value obtained by the method outlined above corresponds really to the crystal thickness (L_c), or to the thickness of the amorphous layers (L_a). This is a direct consequence of Babinet's theorem. This uncertainty could theoretically be solved, had we obtained an independent knowledge of the absolute crystallinity of the sample and of the thickness of the density transition layers. Unfortunately, there are many pitfalls in the exact determination of the crystallinity of PET samples as is evident from an inspection of literature results on PET crystallinity [18–23]. Large discrepancies exist among authors, sometimes due to differences in the selected method of determination, or to inappropriate hypotheses (e.g., the annealing temperature independence of the density of the crystalline and amorphous regions of PET). Part of the problems could also be due to different contents of iso- and terephthalate moeities in the polymer. Two careful studies combining various experimental techniques (including SAXS absolute intensity and density measurements) even led to opposite conclusions [18, 19]. In the first of these studies, the authors [18] considered that $L_c > L_a$, and, as a consequence, the density of the amorphous regions in the semi-crystalline sample (ρ_{ac}) was computed to be smaller by as much as 0.05 g cm^{-3} than in a pure amorphous sample (ρ_{a0}). Fischer et al. [19], on the other hand, considered $L_c < L_a$, and ρ_{ac} was consequently computed to be slightly larger than ρ_{a0}, which is more in accordance with intuitive expectations. For PEEK, we demonstrated elsewhere [24] that the density of the amorphous regions is indeed slightly larger in the semi-crystalline samples than in the pure amorphous polymer, and that the crystal thickness is reasonably estimated by the method outlined above. The consistency of our conclusions was confirmed by a study of the morphology of PEEK/poly(ether imide) miscible blends, where the evolution of the thickness of the crystals and amorphous layers could be followed as a function of the PEI content. Given the similarity between PEEK and PET, it is very likely that ($\rho_{ac} > \rho_{a0}$) for PET as well; this implies in turn that $L_c < L_a$, as is the case with the way we determine L_c in the present paper. However, complementary experiments in this field are clearly required to settle the issue definitively.

Results and discussion

In order to distinguish the structural variations due to reversible effects, such as thermal expansion, from those due to real morphological changes, cyclic {heating-cooling} experiments were conducted on initially amorphous samples.

The following thermal cycle was performed. An initial amorphous sample was heated to 150 °C, held 30 min, and cooled to below T_g (40 °C); the sample was then heated to 200 °C, held 25 min and then cooled to 40 °C. Finally, the sample was heated to 250 °C (above the onset of the final melting peak). All heating and cooling ramps were set at 3 °C min^{-1}.

The heating thermograms of a PET sample subjected to this thermal cycle are presented in Fig. 1. The polymer crystallizes during the first scan at about 130 °C. In the next two heating scans, a small melting endotherm is observed just above the prior annealing temperature (T_c). In the last scan, a large melting endotherm is seen between 225° and 265 °C. This endotherm would have been observed in the other scans as well, had they not been stopped at the selected T_c's [9, 10]. This double melting behavior of cold-crystallized PET is well-known: a similar behavior is exhibited by many other aromatic polymers including poly(phenylene sulphide) and various poly(ether ketones).

The evolution of the long period (L) during this thermal cycle is shown in Fig. 2. L is indicated by circles and squares whereas the temperature cycling is shown by the solid line. In this and the following graphs, filled circles always refer to heating ramps, open circles to cooling ramps, and crossed squares to isotherms. The long period first decreases during the initial crystallization which occurs during heating; then, upon successive cooling and heating, L decreases and increases regularly. The right-hand side of Fig. 2 shows the same data as a function of temperature. This representation is very informative because it allows one to readily separate reversible effects from actual morphological changes. Referring to the results previously acquired on PEEK [1], the data consist of an irreversible branch onto which less sloped reversible branches are grafted. On the reversible branches are points acquired when the sample was cooled and heated below its last highest annealing temperature. The variations along these branches are solely due to thermal expansion and related reversible phenomena. The points on the irreversible branch correspond to the data acquired during crystallization, or during melting-recrystallization when heating the sample above its prior highest annealing temperature. The irreversibility of the evolution of the structural parameters on this branch is indicated of real morphological changes.

Similar representations of results are shown in Figs. 3–6 for the invariant Q, the average lamellar thickness (L_c), the average thickness of the

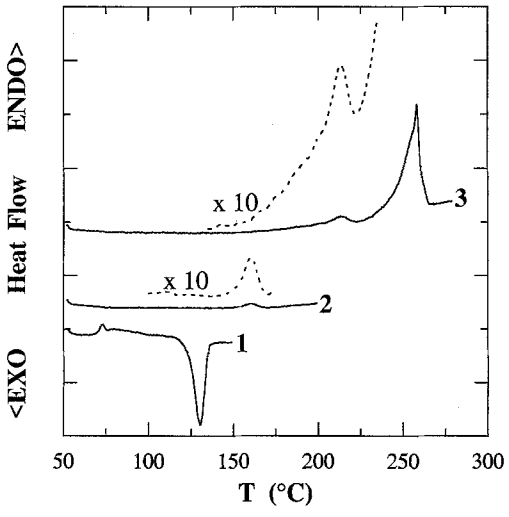

Fig. 1. DSC heating thermograms at 3 °C min^{-1} of an initially amorphous PET sample successively annealed at higher temperatures (see text). First trace: initial amorphous sample; second trace: previous sample, annealed for 30 min. at 150 °C; third trace: previous sample, annealed for 25 min. at 200 °C

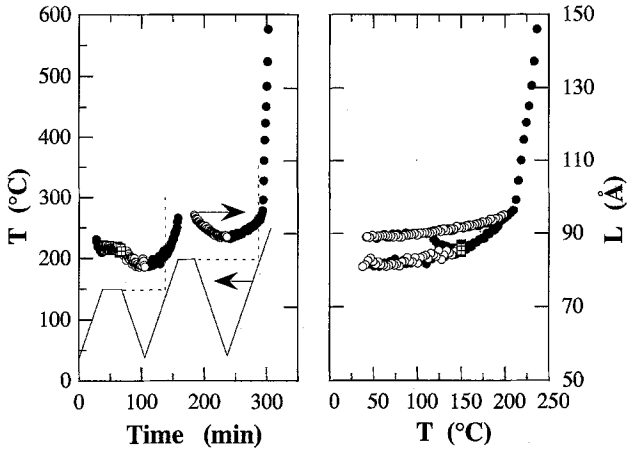

Fig. 2. Left: time evolution of the temperature (continuous line) and of the SAXS long period (L) of a PET sample subjected to heating/annealing/cooling cycles with increasing annealing temperatures. Right: the same data, plotted as a function of temperature. Symbols: Filled circles refer to heating sections, open ones to cooling sections, and crossed squares to annealing sections

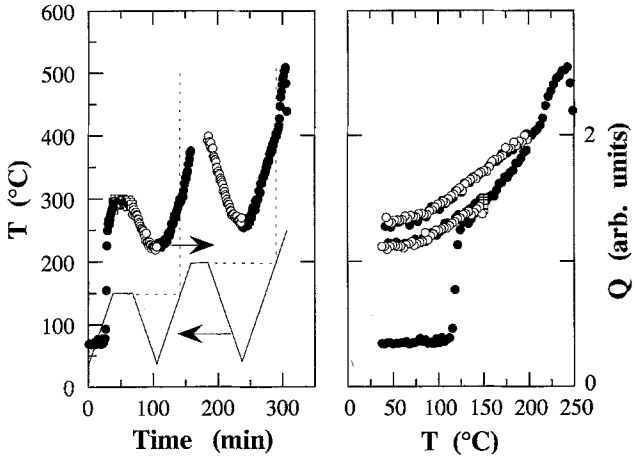

Fig. 3. Left: time evolution of the temperature (continuous line) and of the SAXS invariant (Q) of a PET sample subjected to heating/annealing/cooling cycles with increasing annealing temperatures. Right: the same data, plotted as a function of temperature. Symbols: Filled circles refer to heating sections, open ones to cooling sections, and crossed squares to annealing sections

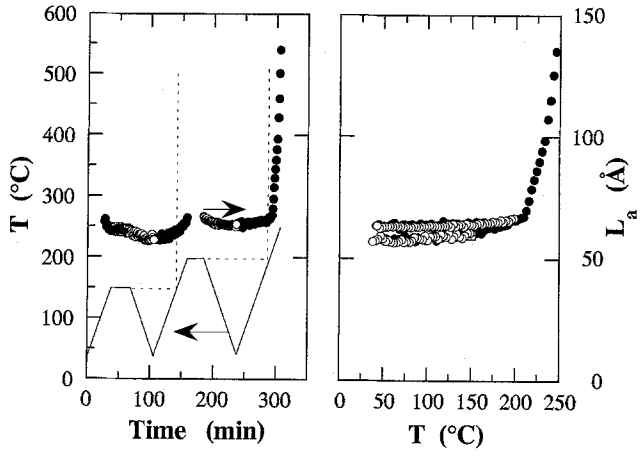

Fig. 5. Left: time evolution of the temperature (continuous line) and of the average thickness of the amorphous layers (L_a) of a PET sample subjected to heating/annealing/cooling cycles with increasing annealing temperatures. Right: the same data, plotted as a function of temperature. Symbols: Filled circles refer to heating sections, open ones to cooling sections, and crossed squares to annealing sections

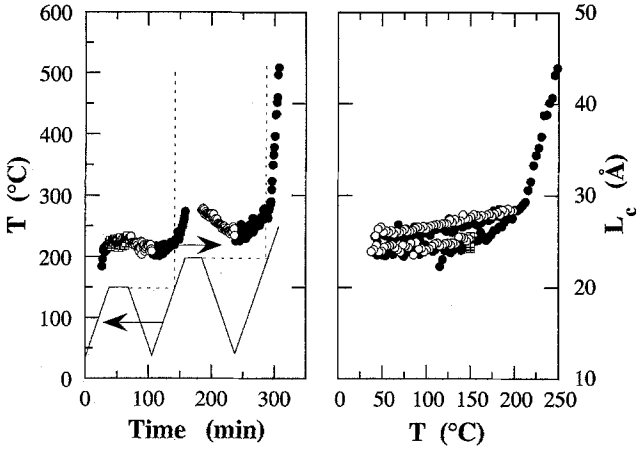

Fig. 4. Left: time evolution of the temperature (continuous line) and of the average crystal thickness (L_c) of a PET sample subjected to heating/annealing/cooling cycles with increasing annealing temperatures. Right: the same data, plotted as a function of temperature. Symbols: Filled circles refer to heating sections, open ones to cooling sections, and crossed squares to annealing sections

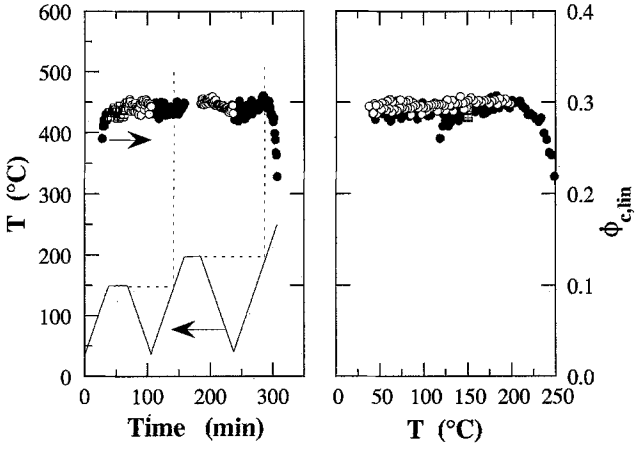

Fig. 6. Left: time evolution of the temperature (continuous line) and of the linear crystallinity ($\phi_{c,lin}$) of a PET sample subjected to heating/annealing/cooling cycles with increasing annealing temperatures. Right: the same data, plotted as a function of temperature. Symbols: Filled circles refer to heating sections, open ones to cooling sections, and crossed squares to annealing sections

amorphous layers (L_a) and the linear crystallinity ($\phi_{c,lin}$), respectively. In each figure, reversible and irreversible branches are present. The following observations can be made:

Below the last highest annealing temperature T_c, all structural parameters remain on a reversible branch whose location is determined by T_c. The morphology of the samples is unchanged below T_c.

As soon as the temperature goes above T_c, structural changes occur immediately. Below 215 °C, these changes are characterized by an

increase of the long period, of the invariant, and of the average thickness of the crystalline lamellae and amorphous layers. However, the linear crystallinity changes only slightly, since changes in L_c and L effectively cancel each other. This near-invariance of $\phi_{c,lin}$ with T_c has been reported by others for PET [17, 18]. It is interesting to note that the bulk crystallinity of PET crystallized to completion was also found by some authors [19] to vary only moderately with annealing temperature (between about 0.3 and 0.4). The general observations are similar to those made previously on PEEK [1]. From 215 °C on, the long period and crystal thickness start to increase dramatically, and the linear crystallinity decreases significantly. While the invariant increases, its rate of increase diminishes and above 240 °C it decreases as the final melting occurs. Although no WAXS data have been acquired on PET in this work, SAXS already provides hints that the densification of the crystals observed for PEEK at temperatures above T_c also occurs for PET. This can be noted from the fact that, between 215° and 235 °C, the invariant increases still faster than on the reversible branches despite a significant decrease of the linear crystallinity. We conclude therefore that either the volume of lamellar stacks in the material (ϕ_s), or the density difference between the crystalline and amorphous regions ($\rho_c - \rho_a$), increase faster than attributable to reversible effects alone (cfr eq. 1, neglecting the small variations of d). If the lamellar stacks are volume-filling at the end of the initial crystallization, as they are for PEEk [1], then ϕ_s cannot increase during the subsequent heating scans. Then part of the changes of the invariant above 215 °C must be due to an increasing density difference. If the lamellar stacks are not volume-filling, an increase of ϕ_s with temperature at relatively low temperature could be considered; however, it is every unlikely that ϕ_s could increase near the final melting point, for a sample slowly heated from the glass. Therefore, the experimental results suggest that $(\rho_c - \rho_a)$ of PET increases above T_c faster than expected from reversible effects alone. Note also that since the linear crystallinity increases only very little between 150° and 215 °C, while the invariant increases irreversibly, it is possible that $(\rho_c - \rho_a)$ also increases over this temperature range, unless ϕ_s increases significantly, which is unexpected. It is more likely that the irreversible crystal densification observed by WAXS for PEEK heated above its last highest annealing temperature also occurs in PET.

Different values have been reported for the crystal density of PET in the literature [25]. Small differences in the crystallographic interplanar distances have been observed as a function of crystallization or annealing temperature [19, 26, 27]; however, in contrast with PEEK [1, 28], these variations are small and essentially limited to low crystallization temperatures. Nevertheless, as pointed out by Fischer et al. [19, 29], the relevant parameter to be used in computation of the SAXS invariant is the effective crystal density ρ_c^*. This effective density is the average crystal density computed by including lattice vacancies introduced by the grain boundaries of the mosaic blocks making up the lamellae. As was demonstrated by these authors, ρ_c^* increases with increasing crystallization temperature, following a parallel increase of the size of the mosaic blocks. A very similar observation was made by Konrad and Zachmann [18]. Hence, there is little doubt that a crystal densification occurs upon annealing cold-crystallized PET samples. It has also been demonstrated that ρ_a is slightly different in semicrystalline PET and in pure amorphous PET [16, 18, 19]. Therefore, the determination of crystallinity from density measurements should be considered with caution. Some of the discrepancies reported in the literature when comparing measured and computed SAXS invariants [17] could be due to the neglect of such effects.

A small decrease of the long period can be detected during the crystallization of the initial amorphous sample in the present study (Fig. 2). However, because the initial crystallization does not occur isothermally, it is not feasible to draw definite conclusions concerning the crystallization mechanism from our data alone. A decrease of the long period during isothermal crystallization has been observed by Elsner et al. [2, 3] on unoriented and oriented PET. Similar observations were made on PEEK [1, 5, 7] and other polymers [6], and were usually taken as originating from the progressive insertion of lamellae between existing lamellae. A slight increase of lamellar thickness is discernible in the early stages of the crystallization, though the uncertainty in our estimated values prevents us from being positive on this point.

Below T_c, only reversible effects occur. We have shown for PEEK that these effects result not only from variations in the amplitude of atomic vibrations, but also from a reversible variation of the strains induced in the crystals by their coupling to amorphous regions. A similar conclusion was drawn by Kilian et al. [27] on PET from the evolution of a WAXS crystallinity index with temperature. In the present case, our data confirm that thermal expansion and related reversible phenomena are mainly responsible for the observed variations. For the sake of completeness, it is appropriate to note that Gehrke et al. [4] detected the existence of premelting just before T_c on cold-crystallized PET samples. However, the amount of premelting was very small, despite the high value selected for T_c (225 °C). It is thus evident that premelting, if any, is of very little importance.

Above T_c, the variations observed are compatible with the melting-recrystallization mechanism, also proposed to explain the scattering results on PEEK, and considered for a long time now to be the origin of the double melting behavior of cold-crystallized PET [9, 10]. The entire structure changes rapidly towards stacks of thicker crystals, separated by larger distances, and, as explained previously, probably of increased average density. The data are most interesting above 215 °C, close to the final melting of PET (which begins around 225 °C as determined by DSC). This is because the equivalent range of supercoolings was not available to us in our previous study on PEEK. In this region, PET is developing its final melting endotherm. The increasing lag between the melting of some lamellar stacks and their recrystallization in stacks of thicker lamellae implies that some of the lamellae do not have enough time to form in the new stacks. Hence, the linear crystallinity decreases, as the insertion mechanism which characterizes the crystallization is not rapid enough. The dramatic increase of the long period is thus a kinetic effect. It is indeed not observed when PET samples are given enough time to complete recrystallization [21]. Above 235 °C, some whole stacks are not recrystallizing within the experimental time scale, and one observes the decrease of the invariant that signals the dominance of melting over recrystallization (ϕ_s decreases).

Conclusions

The results of the present work indicate that the mechanisms governing the cold-crystallization of PET and the subsequent evolution of its morphology upon heating are identical to those found for PEEK subjected to similar conditions. The data are consistent with an initial crystallization process occurring through progressive insertion of new lamellae between existing ones, these new lamellae being of similar thickness as the previous ones. No structural changes could be observed below the prior highest annealing temperature T_c. However, above T_c, a rapid continuous melting-recrystallization of the lamellae occurs. This mechanism does not appreciably increase the crystallinity of the samples, but rather increases the thickness of the lamellae and $(\rho_c^* - \rho_a)$. This increase in $(\rho_c^* - \rho_a)$ could arise in part from an improved crystal chain packing, resulting from a decrease of the average strains in the lamellae, as was demonstrated for PEEK [1]. It could also arise in part from an increase of the size of the mosaic blocks making up the crystalline lamellae. More experiments are required to confirm these points.

Surprisingly, throughout the entire temperature range up to the melting point around 250 °C, the crystal core thickness remains quite small, less than ca. 50 Å, and the linear crystallinity of the lamellar stacks remains nearly constant around 0.3. Obviously, because of the various approximations made, the absolute values of these parameters should be considered with some caution. Still, the general trends are clear and supported by results obtained in other works [19, 29]. Such a low crystallinity indicates the presence of thick order-disorder interfacial layers [30, 31] on the lamellar surface, whose thickness increases with temperature. The origin of such a behavior, also found for PEEK, may be related to the presence of stiff aromatic groups in the chain backbone, which makes it more difficult to dissipate the crystalline order in the interfacial region [32]. As the packing improves with increasing crystallization temperature, it would require thicker interfacial regions for the crystalline order to be dissipated, consistent with experimental results in Fig. 5.

Acknowledgments

The authors are indebted to Dr. D. Daoust and Mrs. C. Fagoo for the determination of the PET molecular masses. AJ wishes to express his gratitude to IBM Belgium for its financial support of this work, NATO for a research fellowship, and the U.S. Government for the award of a Fulbright-Hays research scholar grant-in-aid. TPR acknowledges the partial support of Department of Energy, Office of Basic Energy Sciences under contract FG03 88ER 45375. This work was performed in part at the Stanford Synchrotron Radiation Laboratory which is partially supported by the Department of Energy Office of Basic Energy Sciences.

References

1. Jonas A, Russell TP, Yoon DY submitted to J Polym Sci: Polym Phys Ed
2. Elsner G, Zachmann HG, Milch JR (1981) Makromol Chem 182:657
3. Elsner G, Koch MHJ Bordas J, Zachmann HG (1981) Makromol Chem 182:1262
4. Gehrke R, Riekel C, Zachmann HG (1989) Polymer 30:1582
5. Wang J, Alvarez M, Zhang W, Wu Z, Li Y, Chu B (1992) Macromolecules 25:6943
6. Zachmann HG, Wutz C (1993) In: Crystallization of Polymers; Dosière M ed.; NATO ASI Series C, Vol. 405: p. 403
7. Hsiao BS, Gardner KH (1993) In: Crystallization of Polymers; M. Dosière, ed.; NATO ASI Series C, Vol. 405: p. 415
8. Krüger KN, Zachmann HG (1993) Macromolecules 26:5205
9. Holdsworth PJ, Turner-Jonas A (1971) Polymer 12:195
10. Lin S-B, Koenig JL (1984) J Polym Sci: Polym Symp 81:121
11. Russell TP In: Handbook on Synchrotron Radiation, Vol. 3, Brown G, Moncton DE eds, Elsevier Science Publishers (1991), p. 379
12. Koberstein JT, Morra B, Stein RS (1980) J Appl Crystallogr 13:34
13. Strobl GR, Schneider M (1980) J Polym Sci: Polym Phys Ed 18:1343
14. Groeninckx G, Reynaers H, Berghmans H, Smets G (1980) J Polym Sci: Polym Phys Ed 18:1311
15. Groeninckx G, Reynaers H (1980) J Polym Sci: Polym Phys Ed 18:1325
16. Bornschlegl E, Bonart R (1980) Colloid Polym Sci 258:319
17. Santa Cruz C, Stribeck N, Zachmann HG, Balta Calleja FJ (1991) Macromolecules 24:5980
18. Konard G, Zachmann HG (1971) Kolloid Z Z Polym 247:851
19. Fischer EW, Fakirov S (1976) J Mater Sci 11:1041
20. Gehrke R, Zachmann HG (1981) Makromol Chem 182:627
21. Fontaine F, Ledent J, Groeninckx G, Reynaers H (1982) Polymer 23:185
22. Yagpharov M (1982) J Thermal Anal 23:111
23. Rabiej S, Wlochowicz A (1990) Angew Makromol Chem 175:81
24. Jonas AM, Russell TP, Yoon DY submitted to Macromolecules
25. Brandrup J, Immergut EH 'Polymer Handbook' 3rd edition, J Wiley & Sons, New York (1989)
26. Fakirov S, Fischer EW, Schmidt GF (1975) Makromol Chem 176:2459
27. Kilian HG, Halboth H, Jenckel E (1960) Kolloid Z Z Polym 172:166
28. Hay JN, Langford JI, Lloyd JR (1989) Polymer 30:489
29. Fakirov S, Fischer EW, Hoffmann R, Schmidt GF (1977) Polymer 18:1121
30. The order-disorder interfacial layer should not be confused with the density transition layer, which is rather thin.
31. Mandelken L (1990) Accounts Chem 23:380
32. Kumar SK, Yoon DY (1989) Macromolecules 22:3458

Received May 30, 1994;
accepted July 1, 1994

Authors' address:

Dr. Do Y. Yoon
IBM Almaden Research Center
650 Harry Road
San Jose, California 95120, USA